Chinese Chemical Letters 37 (2026) 111358

Contents lists available at ScienceDirect

Chinese Chemical Letters

journal homepage: www.elsevier.com/locate/cclet

Photochemistry regulated fluorescent dyes for real-time tracing subcellular migration in living cells

Ao Wang[a], Ding-Heng Zhou[a], Hong Zhang[a], Xing Zeng[a], Nan Wang[b], Ming-Yu Wu[a], Xiao-Qi Yu[b], Kun Li[a,*], Shan-Yong Chen[a,*]

[a] Key Laboratory of Green Chemistry and Technology of Ministry of Education, College of Chemistry, Sichuan University, Chengdu 610064, China
[b] Department of Chemistry, Xihua University, Chengdu 610039, China

ARTICLE INFO

Article history:
Received 4 March 2025
Revised 18 May 2025
Accepted 22 May 2025
Available online 23 May 2025

Keywords:
Xanthone
Dual-color fluorescence
Photoconvertible probes
Oxygen direct arylation
Multiple subcellular organelles imaging

ABSTRACT

Probes that can undergo photoconversion *in situ* within cells are advantageous tools for live cell imaging in terms of precise spatial and temporal control. We herein present a new concept to construct photoconvertible probes based on intramolecular oxygen direct arylation within cells. Xanthones bearing aryls (XO-Ars) were designed and prepared. XO-Ars undergo oxygen direct arylation under visible light irradiation in cells to afford xanthene derivatives (XE-Ars). XO-Ars initially accumulate in the endoplasmic reticulum (ER) with green emission and then migrate to the mitochondria with bright red emission. Sequential single-cell lighting up experiments show high spatiotemporal control ability and utility in single or multi-cell tracking. In addition, the photoproducts irradiated with optimized wavelength light source show excellent photodynamic therapy effects. As the duration of light exposure increases, the cells begin to undergo apoptosis. These innovative photoconvertible probes capable of migrating from ER to mitochondria driven by light provide a feasible approach for the *in-situ* monitoring of subcellular physiological events and cell apoptosis.

© 2025 Published by Elsevier B.V. on behalf of Chinese Chemical Society and Institute of Materia Medica, Chinese Academy of Medical Sciences.

Subcellular organelles, serving as the fundamental components within cells, play an indispensable and significant role in various biological processes [1–3]. These organelles spatially arranged within the cell exhibit unique functions. For example, the mitochondrion is the cell's energy powerhouse, while the endoplasmic reticulum (ER) is associated with myriad cell events ranging from protein processing, folding and trafficking to metabolism and ion storage [4–8]. In addition, they also engage in cooperation to form organelle interaction networks for the fulfilment of complex biological events [9–11]. Consequently, the development of fluorescent probes capable of concurrently and distinctly visualizing various organelles is highly in demand. Although, the combination utilization of individual two subcellular organelles-targeted probes can achieve this goal, they suffer from some drawbacks including the tedious staining and washing procedure, potential cross-color interferences and increased cytotoxicity [12,13]. Some single probes targeting multiple organelles with dual-color emissions were developed to address these shortcomings [14–17]. These probes worked well, however, they work based on the inherent differences of subcellular organelles, lacking spatiotemporal controllability. The development of dual-color probes capable of visualizing different organelles in cascade mode with precise manipulation remains greatly challenging.

Photoconvertible fluorescent probes in the visible region are powerful tools for studying biological systems because of their excellent non-invasive spatiotemporal control ability. The discovery of protein Kaede promoted the rapid development of photo-convertible fluorescent proteins (PCFPs) and their application in bioimaging [18,19]. Small molecule based photoconvertible probes, having the advantage of versatility, improved optical properties and clear mechanism, constitute good alternatives to PCFPs and powerful tools for bioimaging. Early photoconvertible small molecular fluorescent probes mainly based on the conversion from non-fluorescent probes into fluorescent probes [20,21]. Dual-color photoconvertible fluorophores (DCPFs), able to convert from a bright emissive form to another with a significant shift in emission, show advantageous potential to track labelled cells with ratiometric signals. Therefore, vast majority of research focuses on the development of DCPFs. The Chenoweth group developed an approach toward DCPFs based on electrocyclization/oxidation of methylated diazaxanthilidene and showed its application in tracking individual biomolecule complexes [22,23]. This transformation was further extended to tetraphenylethylene, cyano-stilbene and

* Corresponding authors.
E-mail addresses: kli@scu.edu.cn (K. Li), chensy@scu.edu.cn (S.-Y. Chen).

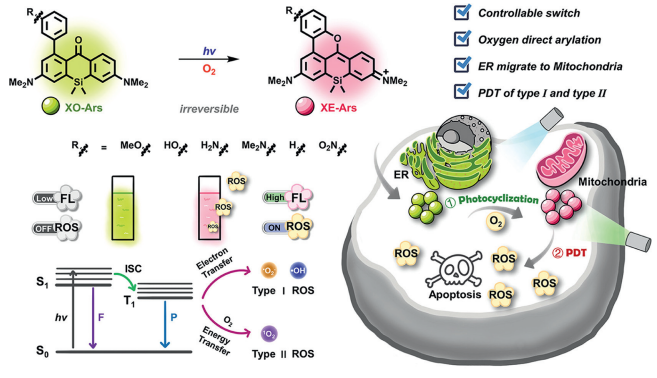
https://doi.org/10.1016/j.cclet.2025.111358
1001-8417/© 2025 Published by Elsevier B.V. on behalf of Chinese Chemical Society and Institute of Materia Medica, Chinese Academy of Medical Sciences.

triphenylphosphindole oxide derivatives, affording several new DCPFs [24–26]. Collot group introduced a new reaction called directed photooxidation induced conversion for the synthesis of DCPFs [27,28]. Other elegant approaches to DCPFs were also proposed based on photoinduced disconnection of oxazine heterocycles and photoextrusion of sulfur monoxide (SO) [29–32]. Recently, the Hell group opened a new way to constitute DCPFs by intramolecular oxygen alkylation [33,34]. Although these works brought new insights into the photoconversion of small fluorophores, and have shown potent application in bioimaging, these DCPFs themselves cannot move from one subcellular organelle to another, impeding their application in multiple subcellular organelles simultaneous imaging.

Subcellular organelle interactions are now attracting increasing attention because they play crucial roles in many cellular functions. Therefore, the development of light-driven DCPFs (LD-DCPFs) with migration ability between subcellular organelles, enabling them to light up multiple subcellular organelles in cascade way has great promise. Moreover, designing new photochemical reactions not only enrich the photochemistry but also offer great opportunities for developing novel photo-responsive biomaterials, especially for those involved reactants and products with markedly different properties.

Herein, we developed a unique oxygen direct arylation reaction for making DCPFs. Xanthones bearing aryls (XO-Ars) undergo oxygen direct arylation under visible light irradiation in cells to afford xanthene derivatives (XE-Ars). XO-Ars initially accumulate in the ER with green emission and then migrate to the mitochondria with bright red emission (Scheme 1). This strategy enables one probe distinctly to visualize two organelles with dual-color emissions in cascade way. Furtherly, photoconversion products XE-Ars show good reactive oxygen generation ability. These LD-DCPFs provide a feasible approach for the *in-situ* monitoring of subcellular physiological events and efficient cell apoptosis.

C–H direct functionalization has been identified as an ideal synthetic approach in organic chemistry owing to its economic steps and environmental friendliness [35–39]. It also provides new opportunities for the designing photoconvertible fluorescent probes. Although various C–H direct functionalization reactions were developed, O-direct arylation without a catalyst has not yet been achieved in organic chemistry, let alone in the field of fluorescent probes. We believe that oxygen direct arylation without a catalyst could be realized with rational structural design. Xanthones bearing aryls (XO-Ars) come into our sight based on the two reasons: (1) The enlarged conjugation structure making the transformation possible; (2) Compounds before and after photoconversion have significant differences in chemical structure, affording markedly different properties (Fig. 1a). To validate our concept, six



Scheme 1. Dual-color photoconvertible probes with light-driven migration ability between organelles.

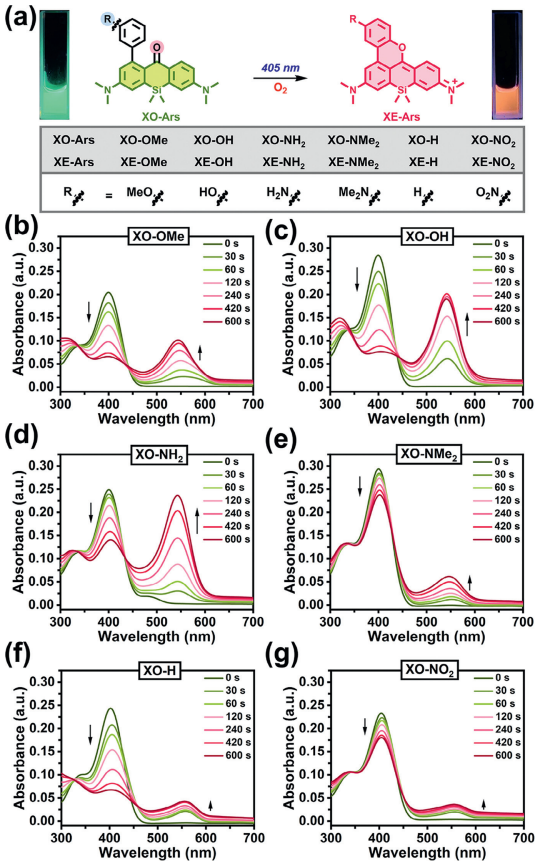


Fig. 1. (a) Photocyclization of six different XO-Ars in the presence of light. (b–g) Changes in absorption spectra of XO–OMe (b), XO–OH (c), XO–NH_2 (d), XO–NMe_2 (e), XO–H (f) and XO–NO_2 (g) under a 460 nm laser (60 mW/cm^2) irradiation condition in an aqueous solution of ACN (ACN/deionized water = 70/30, v/v).

xanthones bearing aryls were designed. The purpose of introducing substituents on the benzene ring is to investigate the influence of electronic effects on the reaction and regulate photoconversion. Brominated xanthones were prepared according to the literature [33], and XO-Ars were prepared by classical Suzuki-Miyaura cross-coupling reaction with good yields (Fig. S2 in Supporting information). With these compounds in hand, we set out to study their photoconversions. At the beginning, we illuminated XO–OMe and XO–OH with four light emitting diode (LED) lights with different wavelengths to filter out the best activation light source (Fig. S5 in Supporting information). The fastest rate of photocyclization of both XO–OMe and XO–OH was achieved under 405 nm LED light. Then, electron effect on the photoconversion was investigated. With the continuous irradiation of the CH_3CN–H_2O solution of XO-Ars, the absorption spectra of all the six compounds gradually decreased, and new bathochromic absorption spectra appeared around 525 nm, indicating the generation of photoconversion products. Generally, electron-rich XO-Ars (XO–OMe, XO–OH, XO–NH_2, XO–NMe_2) have faster photoconversion than electron-neutral (XO–H) or electron deficient (XO–NO_2) XO-Ars (Figs. 1b–e *vs.* Figs. 1f and g).

After investigating the effect of reaction concentrations on the photoconversion efficiency, we found that the lower of the reaction concentration, have the higher photoconversion efficiency (Fig. S6 in Supporting information). Giving the low concentration in living cells, this trend is helpful to photoconversion in cells. Importantly, this photoconvertible probe has good anti-interference ability, which broadens its scope of application within complex biological systems. Common analytes such as amino acids (GSH, Cys, Hcy),

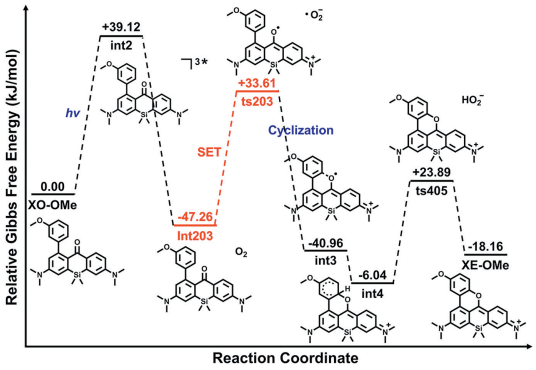


Fig. 2. Proposed mechanism of the photocyclization of XO–OMe and relative Gibbs free energy (kJ/mol) of the reaction.

metal ions (Ca^{2+}, Cu^{2+}, Fe^{2+}, Fe^{3+}, Mg^{2+}, Zn^{2+}), and reactive oxygen species (ROS) ($^{\bullet}O_2^-$, $^{\bullet}OH$, ClO^-, H_2O_2, TBHP, $ONOO^-$) all have little effect on the ring-closing reaction of XO–OMe under light, even if the concentration of these analytes is 100 times that of XO–OMe (Fig. S7 in Supporting information). We further used high performance liquid chromatography (HPLC) to analyze this transformation (Fig. S8 in Supporting information). Apart from the main product, only a small amount of one by-product was observed, indicating that the reaction is clean. To identify the photoconversion products, the product of XO–OMe was isolated with 12.5 % yield and characterized by nuclear magnetic resonance spectroscopy (NMR) and high-resolution mass spectrometry (HR-MS) (Supporting information). The attempt to purify the reaction of XO–OH failed as the photoconversion product XE-OH was liable to air. The photoconversion of XO–OMe under nitrogen atmosphere was obviously retarded compared with that carried out under air atmosphere, indicating oxygen is necessary (Fig. S9 in Supporting information).

Based on the experimental results and literatures, a mechanism (Fig. 2) was proposed to explain this transformation. XO–OMe was initially formed a transition state under photoactivation, and then gave an electron to oxygen to generate a positive radical intermediate. The ring closure and aromatization afforded the photoconversion product XE-OMe. The mechanism was studied with the density functional theory (DFT) method (Fig. 2). The energy barriers for photoexcitation and electron transfer to oxygen are 39.12 and 33.61 kJ/mol, respectively. The two processes determine the reaction rate.

Photophysical properties of XO-Ars and XE-Ars were investigated to provide guidance for the further development of their application potentials. The six xanthones have similar wavelengths both in absorption (around 405 nm) and emission spectra (around 518 nm) and comparable molar extinction coefficients, which showing no matter electron-donating or electron-withdrawing group on the phenyl of XO-Ars have little effect on photophysical properties. XO–H and XO–NO_2 have slow conversion, and the photoconversion products of XO–NH_2 and XO–NMe_2 are dark in aqueous solution. Therefore, their photophysical properties of photoconversion products were not investigated. XE-OMe and XE-OH exhibit high luminescence, with increased quantum yields (5.07 % *vs.* 2.65 % in phosphate buffered saline (PBS), and have large bathochromic-shifts in absorption and emission spectra, affording convenience for dual-color bioimaging (Table 1). The conformations of XO–OMe and XE-OMe in ground state (S_0) are optimized. The highest occupied molecular orbits (HOMOs) distribute on the two-side phenyl ring of the core, and the lowest unoccupied molecular orbits (LUMOs) shift to the middle ring for XO–OMe. While, the LUMOs of XE-OMe shift to both the middle ring and the substituted phenyl. In addition, XE-OMe has decreased E_g compared with XO–OMe, leading to the obvious bathochromic-shifts in absorption spectra (Fig. S10 in Supporting information).

Table 1
Photophysical data of XO-Ars and XE-Ars.

Compound	λ_{abs} (nm)	λ_{em} (nm)	ε (L mol^{-1} cm^{-1}) ($\times 10^4$)	Φ_f (%)
XO–OMe	404	518	2.17	5.07
XO–OH	412	521	2.23	–
XO–NH_2	406	523	1.21	–
XO–NMe_2	406	528	2.14	–
XO–H	408	520	1.67	–
XO–NO_2	408	524	1.72	–
XE-OMe	524	593	2.19	2.65
XE-OH	538	592	–	–

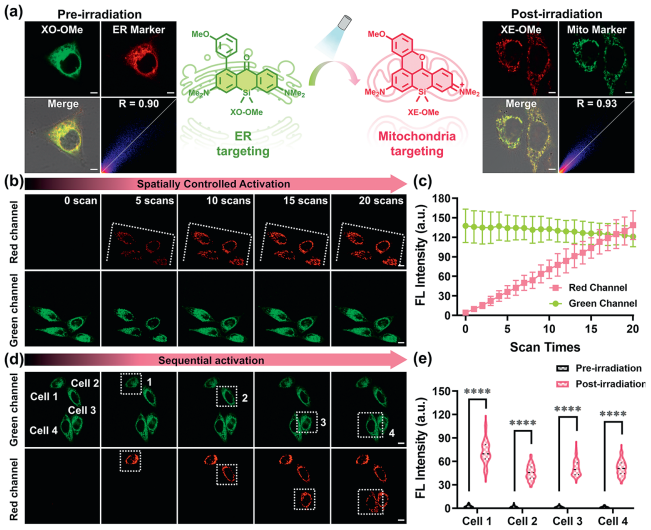


Fig. 3. (a) Co-localization fluorescence imaging of HeLa cells incubated with XO–OMe and ER-Tracker Red, and co-localization fluorescence imaging of HeLa cells incubated with XE-OMe and Mito-Tracker Deep Red FM. (b) CLSM images of HeLa cells treated with XO–OMe (4 μmol/L) taken under laser scanning for 0–20 scans. (c) Average fluorescence intensity of the red and green channels for XO–OMe underwent photoconversion in HeLa cells. (d) Sequential photoconversion photoactivation of 4 μmol/L XO–OMe in individual HeLa cells. Cells 1–4 were sequentially photoconverted at different time points. Green channel: λ_{ex}: 405 nm; λ_{em}: 419–553 nm; Red channel: λ_{ex}: 543 nm; λ_{em}: 593–700 nm; Irradiation laser: 405 nm (2 % power). (e) Fluorescence signal (mean intensity of individual cells) in the XE-OMe (red) channel in HeLa cells ($n = 4$, Student's *t*-test, $^{****}P < 0.0001$. n.s. means no significant difference). Scale bar: 10 μm.

Photoconversion in cells was firstly investigated in HeLa cells incubated with different concentrations (3, 5, 7, 10 μmol/L) of XO–OMe (Fig. S11 in Supporting information). After irradiation with a 460 nm laser (60 mW/cm^2), obvious red emission appeared in cells, showing its high conversion in living cells even in low concentrations. To determine the targeted subcellular organelles, colocalization experiments were conducted. As illustrated in Fig. 3a, XO–OMe had good ER imaging ability before illumination and XE-OMe had excellent mitochondria imaging ability after illumination (Figs. S12 and S13 in Supporting information).

To further illustrate the precise spatial and temporal control ability of this probe, selectively photoactivating cells experiments were performed. Initially, we activated a large population of cells using a 405 nm laser (2 % power). After 20 scans, the mitochondria gradually lit up in the red channel, while the fluorescence intensity of the ER in the green channel decreased with increasing scan cycles (Figs. 3b and c). This gradual "brightening" process is a great way to improve molecular targeting accuracy and signal-to-noise ratio compared to traditional dyes. Secondly, sequentially

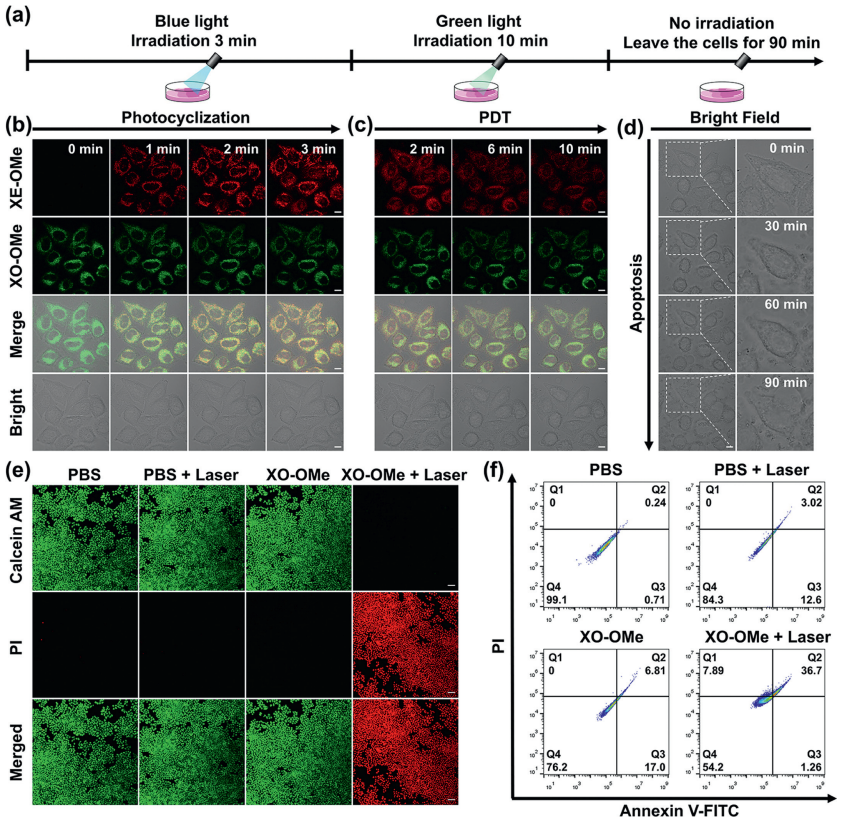


Fig. 4. (a) Schematic representation of the process of incubating HeLa cells with XO–OMe under LED light. (b) CLSM images of HeLa cells treated with XO–OMe (10 μmol/L) taken under a 460 nm laser (60 mW/cm^2) for 3 min. (c) Subsequent confocal images of HeLa cells treated with XO–OMe (10 μmol/L) taken under a 530 nm laser (10 mW/cm^2) for 10 min after the last light (460 nm laser). (d) Real-time images and localized magnified view of HeLa cells treated with XO–OMe (10 μmol/L) taken without irradiation for 90 min after the last light (530 nm laser). (e) Confocal images of HeLa cells with different treatments after being co-stained with calcein-AM (green) and PI (red) for 30 min. (f) Flow cytometry results for XO–OMe induced HeLa cell apoptosis after different treatments. Scale bar: 10 μm.

photoactivating individual cells experiments were carried out. As illustrated in Figs. 3d and e, the four cells in the same field of view were sequentially (1–2–3–4) lit up, and fluorescence intensity in the red region are comparable. These results show this photoconvertible probe XO–OMe has excellent spatiotemporal control ability over individual cells.

Since the whole photoconversion process involves light, we conjectured whether the probe would produce ROS during this light exposure, providing an approach toward photodynamic therapy. Thus, the ROS generation capacity of XE-OMe in aqueous solution was evaluated. Firstly, 2,7-dichlorodihydrofluorescein (DCFH) was adopted as the general ROS indicator. Under a 530 nm LED light (10 mW/cm^2), the fluorescence intensity of DCF gradually increased and enhanced about 680-fold within 180 s, showing excellent ROS generation ability (Fig. S14 in Supporting information). 9,10-Anthracenediy-bis(methylene)di-malonic acid (ABDA) and dihydrorhodamine 123 (DHR123) were used to distinguish the types of ROS. Under a 530 nm LED light (10 mW/cm^2), the absorption peak of ABDA decreased significantly in the presence of XE-OMe (Fig. S15 in Supporting information). Meanwhile, the emission peak of DHR123 had an obvious increasing trend under identical conditions (Fig. S16 in Supporting information). Moreover, hydroxyphenyl fluorescein (HPF) was utilized to further determine the type of free radical. Under a 530 nm LED light (10 mW/cm^2), the fluorescence intensity of HPF remarkably increased in XE-OMe solution and continually enhanced about 85-fold within 600 s (Fig. S17 in Supporting information). These results revealed that $^1O_2$, $^{\bullet}O_2^-$ and $^{\bullet}OH$ could be simultaneously generated. In addition, the presence of $^1O_2$, $^{\bullet}O_2^-$ and $^{\bullet}OH$ was confirmed by the trapping agents 2,2,6,6-tetra-methyl-piperidine (TEMP) and 5,5-dimethyl-1-pyrrolidine-*N*-oxide (DMPO), respectively, through electron paramagnetic resonance (EPR). As shown in Fig. S18 (Supporting information), the characteristic triple peaks of singlet oxygen and the characteristic quadruple peaks of free radicals were recorded after light irradiation, verifying the generation of type I and type II ROS. Thus XE-OMe can act as type I and type II photosensitizers for photodynamic therapy in normoxic and hypoxic environments.

Since XO–OMe is readily activated for photoconversion with a confocal laser in HeLa cells, we opted to use two LED lamps with significantly lower optical power density for cell illumination (Fig. 4a). Clear photoconversion of XO–OMe to XE-OMe was observed in HeLa cells when illuminated with a 460 nm LED light (60 mW/cm^2) (Fig. 4b). Subsequently, a 530 nm LED light (10 mW/cm^2) was used to induce XE-OMe to produce ROS (Fig. 4c). After leaving the cells in darkness for approximately 90 min, a clear trend of cell death was evident (Fig. 4d). This demonstrates that newly generated XE-OMe, following the photoconversion of XO–OMe, can effectively produce reactive oxygen species and induce cancer cell death when stimulated by the corresponding wavelength. This phenomenon confirms that targeting mitochondria with XE-OMe, in combination with photodynamic effects, can enhance the effectiveness of ROS in exerting a killing effect.

To evaluate the biosafety and anticancer potential of XO–OMe and XE-OMe, their cytotoxicity was assessed using the cell counting kit-8 (CCK-8) assay under both dark and illuminated conditions (Figs. S19 and S20 in Supporting information). Under dark conditions, XO–OMe demonstrated negligible cytotoxicity even at high concentrations, suggesting its excellent biocompatibility (Fig. S19). Notably, XE-OMe exhibited significant phototoxicity at a concentration of 4 μmol/L, which was attributed to its efficient generation

of reactive oxygen species (Fig. S20). This study confirmed that the newly formed photoproduct, XE-OMe, following photocyclization under light irradiation, possesses exceptional phototoxicity, providing a promising strategy for future photodynamic therapy applications. These results show that XO–OMe may also serve as a prodrug activated spatiotemporally by light.

Furthermore, cell viability testing was clearly visualized by confocal laser scanning microscopy (CLSM) with calcein-AM (green, a marker for live cells) and propidium iodide dyes (PI, red, a marker for dead cells). The images of CLSM showed that a view of red PI fluorescence was observed only when HeLa cells were treated with 20 μmol/L XO–OMe upon LED light (initially at 460 nm, 60 mW/cm^2, for 3 min, followed by 530 nm, 10 mW/cm^2, for 10 min), but in other 4T1 cells with treatment of PBS, PBS with LED and XO–OMe, just a green Calcein-AM fluorescence emission could be observed (Fig. 4e). The results indicated that XO–OMe undergoes photocyclization in the light and further leads to cell death and photodynamic therapy acted through the apoptotic pathway according previous reports. In order to verify the cell death pathway, the flow cytometry experiments with Annexin V-FITC/PI dyes were carried out. As exhibited in Fig. 4f, the cell apoptosis ratio was up to 36.7 % after treatment with XO–OMe and LED light irradiation. Nevertheless, the percentage of other group was sharply decreasing (0.24 % for PBS, 3.02 % for PBS + laser, and 6.81 % for XO–OMe), which was similar with the results of CLSM and CCK-8. In conclusion, XO–OMe not only achieved *in situ* intracellular photocyclization and underwent organelle migration, but also was a pre-drug with excellent photodynamic antitumor properties under light exposure.

Finally, XO–OMe was imaged under a 100× confocal microscope (Fig. 5). The gradually illuminated mitochondria generated by XE-OMe from XO–OMe under laser irradiation were clearly visible through the red channel. After a period of laser irradiation, XE-OMe gradually escaped from the mitochondria into the cytoplasm. We speculate that this may be due to the apoptosis induced by ROS produced by XE-OMe, which subsequently leads to changes in mitochondrial membrane permeability or membrane potential. This facilitates further research into the correlation between apoptosis and mitochondrial changes.

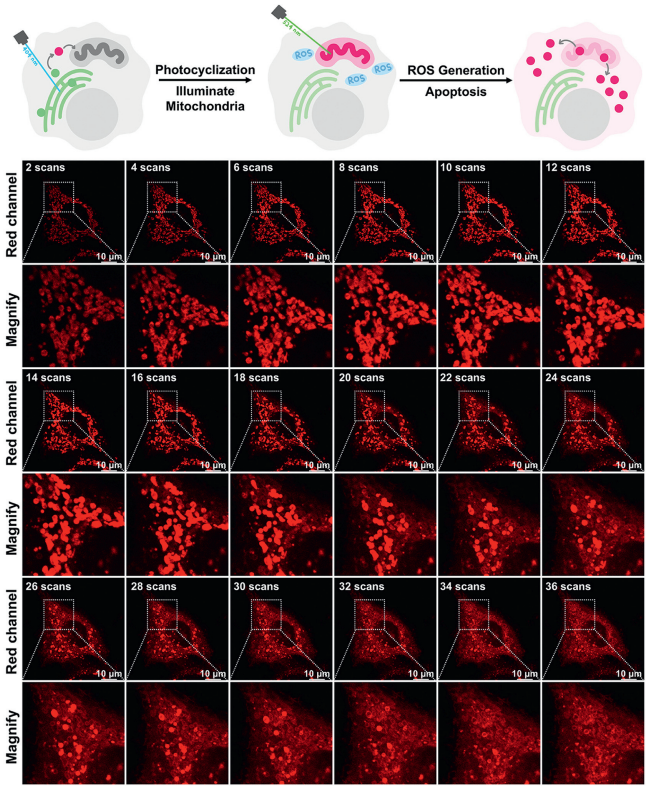


Fig. 5. The association between apoptosis and mitochondrial morphological alterations. Confocal images of HeLa cells stained with XO–OMe (10 μmol/L) under light irradiation (404 and 524 nm lasers of confocal microscope; red channel: $\lambda_{ex} = 524$ nm and $\lambda_{em} = 590–700$ nm).

In conclusion, we reported a novel photo reaction based on oxygen direct arylation and this transformation was successfully applied to construct photoconvertible fluorescent probes. Several xanthones bearing aryls (XO-Ars) underwent oxygen direct arylation to afford xanthene products XE-Ars within cells in the presence of light. XO-Ars were first enriched in the ER and emitted green fluorescence. With the increase of irradiation time, XO-Ars gradually underwent intramolecular ring closure *in situ* in the cell to generate xanthene derivatives (XE-Ars). XE-Ars progressively migrated from the ER to the mitochondria and emitted bright red fluorescence. Sequential and spatial photoconversion was successfully realized in living cells. At this point, by illuminating the photoproducts with an optimal wavelength light source, XE-Ars produce a combination of type I and type II ROS, which further kills the cells. Thus, this study provides an effective reference for the design of future photocyclization molecules and sequential illumination of organelle probes, extending the toolbox of photoconverting dyes for advanced bioimaging applications.

Declaration of competing interest

The authors declare that they have no known competing financial interests or personal relationships that could have appeared to influence the work reported in this paper.

CRediT authorship contribution statement

Ao Wang: Writing – original draft, Methodology, Investigation, Formal analysis, Data curation. **Ding-Heng Zhou:** Software, Methodology, Investigation, Data curation. **Hong Zhang:** Supervision, Resources, Methodology. **Xing Zeng:** Writing – original draft, Project administration, Methodology. **Nan Wang:** Software, Resources, Methodology. **Ming-Yu Wu:** Supervision, Methodology. **Xiao-Qi Yu:** Supervision, Project administration. **Kun Li:** Writing – review & editing, Resources, Project administration, Methodology. **Shan-Yong Chen:** Writing – review & editing, Writing – original draft, Project administration, Methodology, Conceptualization.

Acknowledgments

This work was financially supported by National Natural Science Foundation of China (No. U21A20308) and Foundation from Science and Technology Major Project of Tibetan Autonomous Region of China (No. XZ202201ZD0001G). The authors also thank Yan-Hong Liu from the Comprehensive Training Platform of Specialized Laboratory, College of Chemistry, Sichuan University for sample analysis. We also thank the Analytical & Testing Center of Sichuan University for NMR analysis.

Supplementary materials

Supplementary material associated with this article can be found, in the online version, at doi:10.1016/j.cclet.2025.111358.

References

[1] W. Xu, Z. Zeng, J. Jiang, et al., Angew. Chem. Int. Ed. 55 (2016) 13658–13699.
[2] H. Zhu, J. Fan, J. Du, et al., Acc. Chem. Res. 49 (2016) 2115–2126.
[3] L. Wang, M.S. Frei, A. Salim, et al., J. Am. Chem. Soc. 141 (2019) 2770–2781.
[4] D.S. Schwarz, M.D. Blower, Cell. Mol. Life Sci. 73 (2016) 79–94.

[5] H.M. McBride, M. Neuspiel, S. Wasiak, Curr. Biol. 16 (2006) R551–R560.
[6] C. Ma, F. Xia, S.O. Kelley, Bioconjug. Chem. 31 (2020) 2650–2667.
[7] C. Li, C. Zong, Y. Liu, et al., Chin. Chem. Lett. 35 (2024) 108323.
[8] P. Wang, H. Fang, M. Wang, et al., Chin. Chem. Lett. 36 (2025) 110099.
[9] A.M. Valm, S. Cohen, W.R. Legant, et al., Nature 546 (2017) 162–167.
[10] H. Zhang, L. Shi, K. Li, et al., Angew. Chem. Int. Ed. 61 (2022) e202116439.
[11] J. Ding, R. Xiao, A. Bi, et al., Chin. Chem. Lett. 34 (2023) 108273.
[12] R. Yang, X. He, G. Niu, et al., ACS Sens. 6 (2021) 1552–1559.
[13] L. Guo, M. Tian, Z. Zhang, et al., J. Am. Chem. Soc. 143 (2021) 3169–3179.
[14] W. Ge, H. Wang, X. Wu, et al., Anal. Chem. 95 (2023) 14787–14796.
[15] J. Niu, F. Meng, Q. Hao, et al., Anal. Chem. 94 (2022) 17885–17894.
[16] J. Wang, J.-T. Yan, S.-T. Zeng, et al., Anal. Chem. 95 (2023) 16609–16617.
[17] R. Yang, C. Zhu, X. Yang, et al., Sens. Actuators B: Chem. 424 (2025) 136912.
[18] N.G. Gurskaya, V.V. Verkhusha, A.S. Shcheglov, et al., Nat. Biotechnol. 24 (2006) 461–465.
[19] B. Moeyaert, N. Nguyen Bich, E. De Zitter, et al., ACS Nano 8 (2014) 1664–1673.
[20] T. Kobayashi, T. Komatsu, M. Kamiya, et al., J. Am. Chem. Soc. 134 (2012) 11153–11160.
[21] E.R. Ballister, C. Aonbangkhen, A.M. Mayo, et al., Nat. Commun. 5 (2014) 5475.
[22] M.N. Tran, D.M. Chenoweth, Angew. Chem. Int. Ed. 54 (2015) 6442–6446.
[23] J.V. Jun, C.M. Haney, R.J. Karpowicz, et al., J. Am. Chem. Soc. 141 (2019) 1893–1897.
[24] J. Li, Z. Zhuang, J. Guo, et al., Adv. Sci. 10 (2023) 2305516.
[25] X. Gu, E. Zhao, T. Zhao, et al., Adv. Mater. 28 (2016) 5064–5071.
[26] X. Chen, N. Niu, D. Li, et al., Adv. Funct. Mater. 33 (2023) 2211571.
[27] L. Saladin, V. Breton, O. Dal Pra, et al., Angew. Chem. Int. Ed. 62 (2023) e202215085.
[28] L. Saladin, V. Breton, V.Le Berruyer, et al., J. Am. Chem. Soc. 146 (2024) 17456–17473.
[29] Y. Zhang, K.H. Song, S. Tang, et al., J. Am. Chem. Soc. 140 (2018) 12741–12745.
[30] Q. Gong, X. Zhang, W. Li, et al., J. Am. Chem. Soc. 144 (2022) 21992–21999.
[31] S. Tang, Y. Zhang, P. Dhakal, et al., J. Am. Chem. Soc. 140 (2018) 4485–4488.
[32] Y. Zhang, S. Tang, L. Sansalone, et al., Chem. Eur. J. 22 (2016) 15027–15034.
[33] R. Lincoln, M.L. Bossi, M. Remmel, et al., Nat. Chem. 14 (2022) 1013–1020.
[34] I. Likhotkin, R. Lincoln, M.L. Bossi, et al., J. Am. Chem. Soc. 145 (2023) 1530–1534.
[35] S. Wang, S.Y. Chen, X.Q. Yu, Chem. Commun. 53 (2017) 3165–3180.
[36] G. Song, F. Wang, X. Li, Chem. Soc. Rev. 41 (2012) 3651.
[37] T. Gensch, M.N. Hopkinson, F. Glorius, et al., Chem. Soc. Rev. 45 (2016) 2900–2936.
[38] F. Wang, S. Yu, X. Li, Chem. Soc. Rev. 45 (2016) 6462–6477.
[39] J.R. Hummel, J.A. Boerth, J.A. Ellman, Chem. Rev. 117 (2017) 9163–9227.